

# Reassessment of MIPAS age of air trends and variability

F. J. Haenel<sup>1</sup>, G. P. Stiller<sup>1</sup>, T. von Clarmann<sup>1</sup>, B. Funke<sup>2</sup>, E. Eckert<sup>1</sup>, N. Glatthor<sup>1</sup>, U. Grabowski<sup>1</sup>, S. Kellmann<sup>1</sup>,  
M. Kiefer<sup>1</sup>, A. Linden<sup>1</sup>, and T. Reddmann<sup>1</sup>

<sup>1</sup>Karlsruhe Institute of Technology, Institute for Meteorology and Climate Research,  
Karlsruhe, Germany

<sup>2</sup>Instituto de Astrofísica de Andalucía (CSIC), 18008 Granada, Spain

Correspondence to: F. J. Haenel (florian.haenel@kit.edu)

**Abstract.** A new and improved setup of the SF<sub>6</sub> retrieval together with a newly calibrated version of MIPAS-ENVISAT level 1b spectra (version 5, ESA data version 5.02/5.06) was used to obtain a new global SF<sub>6</sub>-data set, covering the total observational period of MIPAS from July 2002 to April 2012 for the first time. Monthly and zonally averaged SF<sub>6</sub>-profiles were converted into mean age of air using a tropospheric SF<sub>6</sub>-reference curve. The obtained data set of age of air was compared to airborne age of air measurements. The temporal evolution of mean age of air was then investigated in 10° latitude and 1–2 km altitude bins. A regression model consisting of a constant and a linear trend term, 2 proxies for the quasi-biennial oscillation variation, sinusoidal terms for the seasonal and semi-annual variation and overtones was fitted to the age of air time series. The annual cycle for particular regions in the stratosphere was investigated and compared to other studies. The age of air trend over the total MIPAS-period consisting of the linear term was assessed and compared to previous findings of Stiller et al. (2012). While the linear increase of mean age is confirmed to be positive for the Northern mid-latitudes and Southern polar middle stratosphere, differences are found in the Northern polar upper stratosphere, where the mean age is now found to increase as well. The magnitude of trends in the Northern mid-latitude middle stratosphere is slightly lower compared to the previous version and the trends fit remarkably well to the trend derived by Engel et al. (2009). Negative age of air trends found by Stiller et al. (2012) are confirmed for the lowermost tropical stratosphere and lowermost Southern mid-latitudinal stratosphere. Differences to the previous data versions occur in the middle tropical stratosphere around 25 km, where the trends are now negative. Overall, the new latitude–altitude distribution of trends appears to be less patchy and more coherent than the previous one. The new data provide evidence of an accelerating shallow branch of the Brewer–Dobson cir-

ulation, at least in the Southern Hemisphere. Finally the age of air decadal trends are compared to trends calculated with simulated SF<sub>6</sub> values by the Karlsruhe Simulation Model of the Middle Atmosphere (KASIMA) and good agreement is found. The hemispheric asymmetry in the trends found in the MIPAS data are also indicated in the trends calculated with simulated SF<sub>6</sub> values by the KASIMA model.

## 1 Introduction

While it is widely accepted that climate change with enhanced greenhouse-gas abundances leads to a warming of the troposphere and a cooling of the stratosphere, the secondary effects, in particular on the global circulation in the stratosphere, the Brewer–Dobson-Circulation (BDC), are still an issue of current research (Butchart, 2014). A changing BDC will have large impact on the overall composition of the stratosphere, on the ozone budget and distribution (Shepherd, 2008; Li et al., 2009) and on the lifetimes of ozone-depleting substances such as CFCs (Butchart and Scaife, 2001; Douglass et al., 2008) and greenhouse gases. The mean age of air, which is the average transit time of an air parcel from the entry point of the stratosphere, the tropical tropopause, has become a measure for the strength of the BDC in particular for observational analysis (Hall and Plumb, 1994; Waugh and Hall, 2002). The mean age of air comprises both information on the speed of the advection and the amount of mixing and stirring exerted on the air parcel. Modern general circulation models (GCMs) and chemistry-climate models (CCMs) consistently simulate an acceleration of the BDC in a greenhouse gas-induced changing climate (Rind et al., 1990; Butchart and Scaife, 2001; Butchart et al., 2006; Austin and Li, 2006; Garcia and Randel, 2008; Li et al., 2008; Calvo and Garcia, 2009; McLandress and Shepherd, 2009; Butchart et al., 2010;

Okamoto et al., 2011; Bunzel and Schmidt, 2013; Oberländer et al., 2013). So far, however, this expected speeding up of the BDC has not been confirmed by observations. Engel et al. (2009) provided a 30 year record of mean age of air derived from CO<sub>2</sub> and SF<sub>6</sub> balloon-borne measurements which showed a slight but insignificant increase of mean age over the years 1975–2005 for Northern mid-latitudes, which would indicate a decelerated BDC. Bönisch et al. (2011) reported an acceleration of the shallow branch of the BDC for the time period 1979–2009, while they found an unchanged deep branch. Diallo et al. (2012) investigated the age of stratospheric air in the ERA-Interim reanalysis over the period 1989–2010 and stated that the shallow and the deep branch of the BDC may evolve differently. They found a negative and significant age of air trend in the lower stratosphere and a positive but insignificant trend in the middle stratosphere. Stiller et al. (2008, 2012) provided the first global data set on age of air derived from satellite SF<sub>6</sub> measurements. In their paper MIPAS-ENVISAT level 1b spectra of versions 3 and 4 were used to retrieve vertical profiles of SF<sub>6</sub> distributed over the whole globe for the time-period September 2002 to January 2010. Monthly zonal means were converted into mean age of air, from which decadal trends were inferred for latitude and altitude bins.

The derived age of air trends were found to be spatially inhomogeneous with regions of increasing mean age of air and regions of decreasing age of air. The non-homogeneity of trends was also reported by Monge-Sanz et al. (2012), who also found a significant increasing trend in the mean age of air over Northern mid-latitudes in an multiannual CTM simulation driven by ERA-Interim winds over the period 1990–2009 and confirmed the measurements by Stiller et al. (2012) and Engel et al. (2009). In their model study they already noticed a hemispheric asymmetry, which was also later found by Mahieu et al. (2014) with SLIMCAT model calculations. Ploeger et al. (2015) confirmed this hemispheric asymmetry with calculations of the CLaMS model, also driven by ERA-Interim data, and found positive trends in the Northern hemisphere and negative trends in the Southern hemisphere for the time-period 2002–2012.

The work presented here is a continuation of the work of Stiller et al. (2012). An extended and improved SF<sub>6</sub> data set is provided on the basis of a newly calibrated version of MIPAS-ENVISAT level 1b spectra (version 5, ESA data version 5.02/5.06). This new global SF<sub>6</sub>-data set for the first time covers the total MIPAS-period from July 2002 to April 2012.

The characteristics of the MIPAS instrument are presented in Sect. 2. The improvements on the retrieval setup are discussed in Sect. 3. The characteristics and morphology of the new global SF<sub>6</sub>-data set and the resulting age of air data set are assessed in Sect. 4. Then the temporal development is investigated and compared with the previous findings (Sect. 5). In Sect. 6 MIPAS derived AoA trends are compared with trends calculated with simulated SF<sub>6</sub> values from

the Karlsruhe Simulation Model of the Middle Atmosphere (KASIMA). Finally, in Sect. 7, we summarize the lessons learned about possible changes of the BDC.

## 2 MIPAS

MIPAS (Michelson Interferometer for Passive Atmospheric Sounding) is a Fourier transform infrared (FTIR) spectrometer aboard ENVISAT (Environmental Satellite, Fischer et al., 2000) and was designed for the detection of mid-infrared limb emission spectra in the middle and upper atmosphere. The atmospheric spectra were inverted into vertical profiles of atmospheric pressure, temperature and volume mixing ratios (vmrs) of at least 30 trace constituents. Details of the MIPAS instrument can be found in Fischer et al. (2008).

In 2004 the operation of the MIPAS instrument was interrupted due to a problem with the interferometer slide. The optical path difference was then reduced, implying a deterioration of the spectral resolution from 0.025 to 0.0625 cm<sup>-1</sup>. The first phase of the mission (2002–2004) is usually referred to as the MIPAS full resolution (FR) period, while the second phase (2005–2012) is called the reduced resolution (RR) period.

Because of the long optical path through the atmospheric layers, MIPAS could also detect trace gases with very low mixing ratios. Vertical information was gained by scanning the atmosphere at different elevation angles with different tangent altitudes. MIPAS could observe atmospheric parameters in the altitude range from 5 to 160 km with minimum and maximum steps of 1 and 8 km, respectively (Fischer et al., 2008).

## 3 Improvement of the retrieval of SF<sub>6</sub> mixing ratios

Data processing relies on constrained least squares fitting using the Tikhonov (Tikhonov, 1963) regularization approach. Further details of the MIPAS data processor used are described in von Clarmann et al. (2003, 2009). Information on temperature and line of sight, as well as the spectral shift was taken from preceding MIPAS retrievals performed prior to SF<sub>6</sub> in the sequential retrieval chain.

While the retrieval of SF<sub>6</sub> by Stiller et al. (2012) relied on ESA version 4.61/4.62 and 4.67 calibrated radiance spectra, we have used version 5.02/5.06 spectra provided by ESA in the course of reprocessing of the data. These data are considered superior with respect to 4.61/4.62/4.67, in particular because the spectra of the FR period no longer suffered from a calibration insufficiency which was reported as “baseline-oscillations” in Stiller et al. (2008) and the whole data set is better calibrated now. Further technical details on the MIPAS level 1b data can be found at <https://earth.esa.int/web/sppa/mission-performance/esa-missions/envisat/mipas/products-and-algorithms/products-information>.

Beyond this, the SF<sub>6</sub> retrieval setup has been improved over that used by Stiller et al. (2012). Improvements are related to the consideration of non-local thermodynamic equilibrium emission of interfering CO<sub>2</sub> lines, the treatment of interfering species in general, and the details of the joint-retrieval of the background continuum. The implementation of the altitude-dependence of the regularization strength has been slightly changed. The definition of the analysis window (941–952 cm<sup>-1</sup>, see Fig. 1), the regularization strength of the inverse problem, and the spectroscopic database chosen remained unchanged since no improvements over the approach by Stiller et al. (2012) could be achieved with respect to these. Spectroscopic data were used from a dedicated MIPAS database for gases like H<sub>2</sub>O, CO<sub>2</sub>, O<sub>3</sub> and COF<sub>2</sub> (Flaud et al., 2003). For N<sub>2</sub>O, NH<sub>3</sub>, CFC-12 and SF<sub>6</sub> the spectroscopic database HITRAN2000 (Rothman et al., 2003) was used. Tests with varying regularization parameters did not lead to any retrieval improvements, i.e. the regularization strength chosen by Stiller et al. (2012) has been confirmed to be adequate. The new SF<sub>6</sub> data described and used here are version V5h\_SF6\_20 for the FR data product and V5r\_SF6\_222 and V5r\_SF6\_223 for the RR period. The latter two data versions have no discernible differences; their different version numbers just reflect different sources of ECMWF meteorological analysis data used in the retrieval. In the FR V5h\_SF6\_20 data version the artefact of the previous version caused by radiance baseline oscillations in the level 1-data described in Stiller et al. (2008) is no longer an issue and has been totally overcome.

### 3.1 Non-local thermodynamic equilibrium

The Q branch of the  $\nu_3$  band of SF<sub>6</sub> at 947.9 cm<sup>-1</sup> analysed here is strongly superimposed by the CO<sub>2</sub> laser band (00011 → 10001) at 947.74 cm<sup>-1</sup> and lies just above the first hot band (01111 → 11101) line at 947.94 cm<sup>-1</sup> (see Fig. 1). These CO<sub>2</sub> emission bands deviate from local thermodynamic equilibrium (LTE) in the middle atmosphere, particularly during daytime. Stiller et al. (2012) approximated the non-LTE effect by treating the CO<sub>2</sub> laser band and hot band emissions as emissions from different (non-CO<sub>2</sub>) species and by fitting their “virtual abundances” along with the SF<sub>6</sub>-retrieval. While these virtual abundances have no physical meaning, they helped to fairly well model the CO<sub>2</sub> laser band emission and to avoid related spectral residuals and error propagation. Contrary to that, our refined analysis relies on explicit modelling of the non-LTE emissions of the CO<sub>2</sub> laser and hot bands. In the course of a preceding CO retrieval (Funke et al., 2007), the vibrational temperatures of the CO<sub>2</sub> laser band and the hot band were calculated for the actual atmospheric conditions. Since the radiative transfer code used in our retrieval, the Karlsruhe Optimized and Precise Radiative Transfer Algorithm (KOPRA, Stiller, 2000; Stiller et al., 2002; Funke and Höpfner, 2000) supports calculation of non-LTE emissions, these could directly be used for the calculation

of the laser band signal and hot band emissions. This improves considerably the description of the CO<sub>2</sub> emissions and reduces the residuals between the observed and modelled spectra, leading eventually to improved SF<sub>6</sub> results (compare residuals at the position of CO<sub>2</sub> lines in Fig. 2).

### 3.2 Interfering gases

Figure 1 shows the spectral window used for the SF<sub>6</sub> retrieval and the expected spectral contributions of contributing species for MIPAS reduced resolution at 20 km in mid-latitudes for July. The signature of the target species SF<sub>6</sub> (red solid line) is quite weak compared to some of the interfering species. Thus a careful treatment of the interfering species is essential to minimize related error propagation. Since for some of the interfering species no reliable a priori information on their abundances is available, these gases are jointly fitted along with SF<sub>6</sub>. For other interferents, abundance information is available from preceding MIPAS retrievals; however inconsistent spectroscopic data or calibration inconsistencies in the SF<sub>6</sub> analysis window and the interferents’ dedicated analysis windows can cause artefacts when the known abundances are used to model the contribution of these gases in the SF<sub>6</sub> analysis window. Thus, it is occasionally adequate to jointly fit these gases along with SF<sub>6</sub>, too. Stiller et al. (2012) have used abundance information from climatologies or preceding MIPAS retrievals for all interfering species except for CO<sub>2</sub> and H<sub>2</sub>O, which were fitted jointly along with SF<sub>6</sub>. In the new retrieval scheme the trace gases COF<sub>2</sub> and ozone were additionally joint-fitted. This helped to minimize the residual of the fit and also removed a slight tilt of the residual in spectral space. For all gases a first order Tikhonov-type regularisation was chosen, which means that the slope of the profile was forced to some constraint, rather than forcing the profile towards an a priori profile as done in the Optimal Estimation approach. Usually the constant zero profile served as a priori profile and by this way oscillations in the profile are damped and the profile becomes smoother. In the following we present a gas-by-gas discussion of our treatment of all interfering species.

#### 3.2.1 CO<sub>2</sub>

CO<sub>2</sub> is the main contributing gas of all emitters in the SF<sub>6</sub> analysis window (microwindow) used (blue solid lines in Fig. 1). As mentioned above the maximum of the SF<sub>6</sub> spectral signature is just underneath of the wing of a CO<sub>2</sub> laser line. In order to get an accurate value of the SF<sub>6</sub> mixing ratio from radiances emitted in the SF<sub>6</sub> microwindow, a very precise modelling of the CO<sub>2</sub> is crucial. We have used a non-LTE model to account for the CO<sub>2</sub> emissions in the middle atmosphere and fitted it jointly with SF<sub>6</sub>. The first guess profile in the iterative procedure was taken from climatologies (Remedios et al., 2007).

### 3.2.2 H<sub>2</sub>O

A water vapour signature is located near the SF<sub>6</sub> Q branch at 948.26 cm<sup>-1</sup>, so a considerable information crosstalk is expected between the H<sub>2</sub>O and the SF<sub>6</sub> signals. The water vapour profile resulting from the preceding retrieval in dedicated microwindows (prefit) was used as a priori and first guess profile for every geolocation. The regularization strength associated with H<sub>2</sub>O was adjusted such that the correction with respect to the initial H<sub>2</sub>O profile had about 1 to 1.5 degrees of freedom. Basically the profiles have the shape of the prefit profile and only a shift of the prefit profile is allowed. The residual near the water vapour line was not reduced when the regularization for water vapour was relaxed. Variations of the regularization for water vapour or the choice of related a priori (constant zero or water prefit), did not have any discernible effect on the SF<sub>6</sub> retrieval.

### 3.2.3 COF<sub>2</sub>

There is not much vertically resolved information contained on COF<sub>2</sub> in the microwindow, but fitting this trace gas jointly with the target species helped to minimize the residuals. A climatological profile served as a priori and first guess profile since there was no prefit of COF<sub>2</sub> available. The regularization was chosen relatively strong such that the resulting COF<sub>2</sub> profiles have about 1.5 to 3.5 degrees of freedom.

### 3.2.4 O<sub>3</sub>

Like COF<sub>2</sub>, ozone does not contribute much to the signal in the microwindow, but profits from the ozone retrieval existed. Thus, the ozone prefit served as a priori and first guess profiles. Together with the joint fit of COF<sub>2</sub>, the joint fit of ozone helped to remove a tilt in the residual. The regularization applied allowed the ozone profiles to have about 1.5 to 3.5 degrees of freedom.

### 3.2.5 Further species

Profiles of N<sub>2</sub>O, NH<sub>3</sub> and CFC-12 were imported from a climatological database (Remedios et al., 2007). Since the signals of these gases are small, related uncertainties are tolerable.

### 3.3 Background continuum and radiance offset

In the previous SF<sub>6</sub> retrieval by Stiller et al. (2012) background continuum radiation was considered up to an altitude of 33 km. In the atmosphere continuum radiation, i.e. radiation which is only varying very slightly in spectral space (in contrast to spectral lines), is emitted by clouds, dust or other aerosol particles. Also the sum of very far wings of spectral lines, no more accounted for by the line by line calculation, can contribute to the continuum radiation. In general it was assumed that a consideration of continuum radi-

ation above 33 km was not necessary, particularly because there are no aerosol contributions expected above the Junge layer. However, it turned out that fitting continuum radiation up to higher altitudes (50 km) could eliminate an artefact in the retrieved SF<sub>6</sub> profile: while in the retrieval of Stiller et al. (2012) an unexplained local maximum in SF<sub>6</sub> occurred around 36 km in the tropics, this supposedly unphysical feature vanishes completely with the new continuum treatment. This provides evidence that there is additional continuum radiation in the atmosphere which if not accounted for leads to elevated SF<sub>6</sub> mixing ratios, since the SF<sub>6</sub> signature is also of broad band nature. The approach of a joint fit of the continuum radiation up to higher altitudes also helped to improve retrievals of other species. In addition, a recent paper pointed out that there is evidence of aerosol particles even above the Junge layer due to meteoric dust (Neely III et al., 2011). In our retrievals we also fit a constant radiance offset jointly, in order to account for a possible residual shift in radiance due to imperfect radiance calibration. This offset had to be strongly regularized in order to cope with the pronounced linear interdependence of the continuum and offset Jacobians.

### 3.4 Miscellaneous

The consideration of continuum up to higher altitudes allowed the usage of more upper tangent heights. While the previous retrieval setup only used the first 19 out of 27 tangent heights in MIPAS reduced resolution mode, the new setup incorporated information from measurements of 22 tangent heights. This allowed more information from higher altitudes to be gained, i.e. the averaging kernel diagonals increased slightly at higher altitudes. In addition the Root Mean Square (RMS) of the residuals in upper tangent heights decreased. Hence, with the new retrieval setup for the first time it made sense to include 22 tangents height instead of 19. The new mean SF<sub>6</sub> profiles contain more information in the altitude range 40–50 km, show more structure and depend less on the prior information there.

### 3.5 Discussion of the retrieval refinement

In Fig. 2 an example for the residual between measured and simulated spectrum at tangent height 12 (approx. 24 km) of the final retrieval setup (upper panels) and the previous setup (lower panels) is shown. To reduce the noise measured and modelled spectra have been coadded over the period of 1 day. One can see that the residuals improved substantially. Especially the CO<sub>2</sub> lines and the water vapour line (compare with Fig. 1) are fit much better and overall the RMS of the residual has been reduced from about 1.8 to 1.0 nW (cm<sup>2</sup> sr cm<sup>-1</sup>)<sup>-1</sup> in this example. Also a slight tilt of the residual in spectral space was removed. The improvements achieved in the residuals are dependent on altitude and latitude. In Table 1 we present previous and final RMS of the residuals between measured and modelled spectra resolved in latitude bands of

Tangent altitude 12≈24 km			
latitude band	RMS previous	RMS final	rel. improvement
0-30	1.861	1.108	40%
30-60	1.704	1.188	30%
60-90	1.092	1.001	8.3%
-30-0	2.034	1.157	43%
-60- -30	2.361	1.390	41%
-90- -60	2.808	1.871	33%

Tangent altitude 14≈28 km			
latitude band	RMS previous	RMS final	rel. improvement
0-30	1.567	1.003	36%
30-60	1.365	0.909	33%
60-90	1.021	1.001	2%
-30-0	1.786	1.035	42%
-60- -30	1.987	1.229	38%
-90- -60	2.432	1.6841	31%

Tangent altitude 16≈31 km			
latitude band	RMS previous	RMS final	rel. improvement
0-30	1.921	1.040	46%
30-60	1.294	1.025	21%
60-90	1.012	0.946	7%
-30-0	1.971	1.034	48%
-60- -30	1.969	1.117	43%
-90- -60	2.037	1.547	24%

**Table 1.** Previous and final RMS of the residual for tangent altitude 12, 14 and 16 with coadded spectra over one day

30° for our example day for 3 selected tangent altitudes. The relative improvements are largest in the tropics and amount to about 40% and are smallest in the Northern polar stratosphere, where infrared radiances are small, because our example data was a day in boreal winter.

With the new retrieval setup the unexplained “nose”, a local maximum in the tropical SF<sub>6</sub> profiles at 36 km did no longer appear after considering the continuum above the standard altitude of 33 km up to an altitude of 50 km.

The vertical resolution of the new SF<sub>6</sub> data is slightly degraded compared to the previous version and varies now from 4 to 6 km at 20 km, from 7 to 10 km at 30 km and from 12 to 18 km at 40 km altitude, due to the inclusion of more gases in the fit, which was done to achieve a higher accuracy and less systematic errors.

#### 4 The new SF<sub>6</sub> data set and age of air distributions

With the new retrieval setup, the complete set of nominal mode MIPAS data was processed and approx. 2.3 million

SF<sub>6</sub> profiles have been retrieved. The profiles belong to geolocations that cover the whole globe and the full MIPAS period from July 2002 to April 2012, however with several data gaps in between. The single profiles scatter a lot and the noise error is too large (in the order of 20 %) to provide useful age of air information from single profiles. But averaged profiles lead to meaningful SF<sub>6</sub>-profiles.

The new SF<sub>6</sub> data set exhibits similar features as the previous one described in Stiller et al. (2012), e.g. the SF<sub>6</sub>-vmrs are increasing with time at all latitudes. Seasonal influences can be identified, like very low mixing ratios at the end of austral winter in the Southern polar latitudes. A figure showing the time series of SF<sub>6</sub> over latitude is included in the electronic supplement.

#### 4.1 Conversion of SF<sub>6</sub> into age of air

For the calculation of age of air (AoA) from SF<sub>6</sub> abundances a SF<sub>6</sub> reference curve is necessary. The theoretical concept of age of air as derived by Hall and Plumb (1994) requires the knowledge of SF<sub>6</sub> mixing ratios at the entry point into the stratosphere, i.e. the tropical tropopause region, over a long period of time. As pointed out by Stiller et al. (2012) such a long term observational data set is not available. Only ground-based observations can provide the necessary reference data. However, transport times from the surface to the tropical tropopause are somewhat uncertain and can amount from days or even hours (to the top of convection) to weeks or months (to the top of the Tropical Tropopause Layer (TTL)). Using surface data as a reference can imply a high bias in this order of magnitude on the AoA data.

This has to be kept in mind when comparing MIPAS AoA distributions to model data, for which time zero is set by tropopause crossing of the air parcel.

We have constructed the SF<sub>6</sub> reference curve as described in Stiller et al. (2012) using NOAA/ESRL SF<sub>6</sub> data. For the period 1995 to November 2013 smoothed ground based global mean combined flask and in-situ data (Hall et al., 2011) is used while for times before 1995 a linear approximation from Hall et al. (2011) ( $y = 0.125 + 0.215 \times (t - 1985)$ ) is applied. The reference curve is extended with a linear extrapolation until June 2014 to deal with MIPAS SF<sub>6</sub> values slightly higher than the reference values at that certain time that can occur sporadically due to their random errors.

The AoA is then calculated by simply mapping the measured SF<sub>6</sub> value on the reference curve and reading of the reference time. The time difference, the so called lag time approximates the AoA. According to Hall and Plumb (1994) this lag time is only equivalent to the mean age of air, if the used tracer is growing strictly linear, i.e. the reference curve has to be linear. Because our constructed reference curve appears to be slightly non-linear, a correction is applied. Within an iterative procedure the reference curve is convoluted with a typical age spectrum. More details of this non-linearity correction are discussed in Stiller et al. (2012).

SF<sub>6</sub> is a stable tracer in the stratosphere. However, it has a mesospheric sink. Every winter SF<sub>6</sub>-depleted air from the mesosphere subsides into the polar vortex leading to “apparent ages” which are considerably larger than the true ages. This “overaging” is most pronounced in the polar vortices, where AoA derived from SF<sub>6</sub> can be greater by 2 or more years (Waugh and Hall, 2002). However, due to inmixing of some of the vortex air into mid-latitudes, the entire stratosphere is affected to a certain degree. This should be kept in mind when comparing AoA calculated from SF<sub>6</sub> abundances with AoA calculated from other tracers or model studies. Stiller et al. (2012) estimated the global effect of overaging to about 0.08 years per year of age for the Southern Hemisphere and to about 0.04 years per year of age for the Northern Hemisphere.

## 4.2 Global distribution of AoA

The derived monthly zonal means of AoA have a precision in terms of the standard error of the means of 0.06–0.4 years for the reduced resolution period and of 0.08–0.5 years for the full resolution period. Most of the monthly means are composed of 500–800 single values, if fully occupied.

The global distribution of the newly derived AoA data set can be seen as average over all years for the four seasons in Fig. 3.

Highest AoA values occur in the polar stratosphere in hemispheric winter to spring being particularly high in the Southern Hemisphere. This again can be explained by intrusion and subsidence of old upper stratospheric and mesospheric air into the polar vortex. Due to the mesospheric SF<sub>6</sub> sink, this mesospheric air appears even older than it actually is.

The differences in the zonal monthly means of AoA to the previous data set, averaged over all years for the four seasons, are presented in Fig. 4. The main difference to the old data set is that the local minimum of AoA in the tropics around 36 km is no longer present in the new data set. This feature of the old data set has been proven to be a retrieval artefact, which was eliminated by a refined treatment of continuum radiation (see Sect. 3). This artefact triggered an oscillation in lower layers which are no longer present in the new data set. Above 40 km, the air is now found to be younger at almost all latitudes, which appears to be more realistic. The old data version was reported to have a possible high bias of up to 2 years above 35 km, most pronounced at the summer pole due to the simplified approach concerning the non-LTE treatment of interfering CO<sub>2</sub> lines (Stiller et al., 2008). The full non-LTE treatment used for the new data set has removed this systematic uncertainty. In addition, part of the lower AoA in the upper stratosphere is attributed to the revised regularization of the retrieval.

Among studies of AoA (e.g. Stiller et al., 2012; Diallo et al., 2012; SPARC CCMVal, 2010) it became a standard for validation of measured or modelled AoA to compare with

earlier airborne measurements from the 1990s as published by Waugh and Hall (2002) and Hall et al. (1999). Overall this comparison on a latitudinal cross-section at 20 km turns out to be quite similar to the one in Fig. 4 in Stiller et al. (2012): The agreement of MIPAS AoA with the earlier airborne measurements is excellent in the Northern and Southern mid-latitudes, whereas in the tropics and high latitudes MIPAS exhibits higher age. There are only small differences to the comparison with the previous MIPAS AoA version, like the spread of MIPAS AoA in the tropics is lower and the negative peak of low MIPAS AoA at about 30° N is no longer present in the new version. The respective figure is attached in the electronic supplement.

In Fig. 5 MIPAS AoA profiles are compared to airborne AoA profiles (in-situ CO<sub>2</sub> measurements by Boering et al., 1996; Andrews et al., 2001, in-situ SF<sub>6</sub> measurements by Ray et al., 1999 and air sample measurements by Harnisch et al., 1996) for the tropics (5° S), the Northern mid-latitudes (40° N) and the Northern high latitudes (65° N). In the tropics MIPAS AoA is older than in-situ CO<sub>2</sub> and SF<sub>6</sub> measurements at all altitudes. In the Northern mid-latitudes the MIPAS profile fits excellently to the SF<sub>6</sub> in-situ data up to an altitude of 27 km and is older higher up. As expected, in-situ CO<sub>2</sub> measurements provide lower ages, and the AoA from SF<sub>6</sub> air samples by Harnisch et al. (1996) is younger, too. At Northern high latitudes, MIPAS age profiles only fit well to the SF<sub>6</sub> air samples taken from polar vortex air. To illustrate the high seasonality, monthly averaged MIPAS profiles are additionally shown with oldest ages found for January.

## 5 Observed temporal variability for the period July 2002 to April 2012

For the analysis of the temporal variability of the new AoA data set the same methods were applied as in Stiller et al. (2012), i.e. the following regression function was fitted to the data:

$$\text{age}(t) = a + bt + c_1 \text{qbo}_1(t) + d_1 \text{qbo}_2(t) + \sum_{n=2}^9 \left( c_n \sin \frac{2\pi t}{l_n} + d_n \cos \frac{2\pi t}{l_n} \right) \quad (1)$$

where  $t$  is time,  $\text{qbo}_1$  and  $\text{qbo}_2$  are the quasi-biennial oscillation (QBO) indices, and the sum represents 8 sine and 8 cosine functions of the period length  $l_n$ . The period of the first two sine and cosine functions is 12 and 6 month, respectively, representing the seasonal and the semi-annual cycle. The other 6 terms have period lengths of 3, 4, 8, 9, 18 and 24 months and describe deviations of the temporal variation from a pure sine or cosine wave. Fitting sine and cosine of the same period length accounts for a possible phase shift of the oscillation. The terms  $\text{qbo}_1$  and  $\text{qbo}_2$  are the normalized Singapore winds at 30 and 50 hPa as provided by the Free University of Berlin via <http://www.geo.fu-berlin.de/met/ag/>

strat/produkte/qbo/index.html. These QBO-proxies are approximately orthogonal such that their combination can emulate any QBO phase shift (Kyrölä et al., 2010). For the fit of the coefficients  $a, b, c_1, \dots, c_9, d_1, \dots, d_9$  to the data, the method of von Clarmann et al. (2010) is used, which considers the full error covariance matrix of mean age data  $\mathbf{S}_m$  with the squared standard errors of the means (SEM) of the monthly zonal means as the diagonal terms (Stiller et al., 2012).

An example of the fit of our regression model to MIPAS monthly zonal mean data can be seen in the electronic supplement. The fit considers a potential bias of the two MIPAS measurement periods (dashed orange line) as described in von Clarmann et al. (2010). Such a fit is done for every  $10^\circ/1\text{--}2\text{ km}$  latitude–altitude bin.

### 5.1 Age of air trends

In Stiller et al. (2012) the timeseries analysis was first discussed within the framework of descriptive statistics, i.e. without consideration of the autocorrelations in the residuals of the trend analysis. As a second step, the analysis was repeated within the framework of inductive statistics, where autocorrelated model errors have to be considered. In this study we focus on the trend analysis which is referred to as “model-error corrected linear increase” in Stiller et al. (2012), because the analysis without consideration of the autocorrelated model errors leads to very similar trends whose significances, however, are considerably overestimated.

As described in Stiller et al. (2012) our regression model only accounts for the linear trend, several periodics and the QBO-terms. Other atmospheric variability, especially from non-periodic events, is not included in this model. This results in fit residuals which are considerably larger than the data errors represented by the covariance matrix  $\mathbf{S}_m$ , which includes only the standard errors of the monthly means and the correlated terms to account for the possible bias between the MIPAS data subsets (von Clarmann et al., 2010). Therefore the  $\chi_{\text{reduced}}^2$  of the fit with

$$\chi_{\text{reduced}}^2 = \frac{(\mathbf{age}_{\text{MIPAS}} - \mathbf{age}_{\text{modelled}})^T \mathbf{S}_m^{-1} (\mathbf{age}_{\text{MIPAS}} - \mathbf{age}_{\text{modelled}})}{m - n} \quad (2)$$

exceeds the value of unity in most cases, where  $\mathbf{age}_{\text{MIPAS}}$  and  $\mathbf{age}_{\text{modelled}}$  are the data vectors containing the measured and modelled age values, respectively, and where  $m$  and  $n$  are the number of data pairs and the number of fitted coefficients, respectively (Stiller et al., 2012). In order to consider the model errors of the regression model, the autocorrelation of two adjacent data-points was estimated in a first step. In a second step the fit was rerun with the autocorrelation and a constant error term added to the covariance matrices. These additional terms in the covariance matrices were

scaled within an iterative procedure, such that the resulting  $\chi_{\text{reduced}}^2$  of the trend fit was close to unity. This iterative procedure is necessary because the additional autocorrelated error term changes the weight between the data points in the fit.

The linear increase of AoA over the whole MIPAS-period derived from our regression analysis varies with altitude and latitude. The global view can be seen in Fig. 6 top panel. Red areas indicate increasing AoA, while blue regions indicate decreasing AoA. Hatched areas indicate where the trend is not significant, i.e. it is smaller in absolute terms than its  $2\sigma$ -uncertainty.

The overall pattern of linear increase/decrease is in good agreement with the respective picture of the trend fit without consideration of autocorrelation and empirical errors (see respective Figure in the supplement), which confirms that our method is robust. The significance of most data bins is lower, as expected, due to the additional error terms.

The distribution of trends in the latitude–altitude plane roughly confirms the mean trends of those obtained by Stiller et al. (2012) and their general morphology but looks more coherent and less patchy, meaning that regions of linear increase and decrease, respectively, are more contiguous. There are basically two regions of linear decrease: A large one consisting of the tropics and Southern subtropics between about 19 to 30 km and extending to the lowermost mid-latitudinal Southern stratosphere, and a smaller one consisting of the upper tropical troposphere extending to the lowermost stratosphere of mid-latitudes. These regions are surrounded by regions of AoA linear increase. Largest positive linear trends were observed in the polar regions. Compared to findings of Stiller et al. (2012) a positive linear increase of mean age is confirmed for the Northern mid-latitudes and Southern upper polar stratosphere. Negative age of air trends of Stiller et al. (2012) in the lowermost tropical stratosphere and lower Southern mid-latitudinal stratosphere are also confirmed. Differences are found in the Northern polar stratosphere, where the mean age is now increasing as well. In the tropical stratosphere the picture is now almost opposite to the previous data of Stiller et al. (2012) meaning that AoA is increasing where it used to be decreasing and vice versa. These changes are attributed to the more adequate treatment of the background continuum emission in the retrieval and the associated removal of the spurious  $\text{SF}_6$  maximum and subsequent errors. A clear asymmetry between the hemispheres is visible.

The uncertainties (see Fig. 6, bottom panel) are now more realistic, since now an additional model error has been added, however, they are smaller than the ones derived by Stiller et al. (2012), which is attributed to the longer time series, covering now the full MIPAS period, and the fact that the new AoA data set is less noisy than the previous one.

The vertical profiles of AoA linear trends for every other latitude bin are shown in Fig. 7, top panel. Engel et al. (2009) derived a trend of AoA for  $30$  to  $50^\circ\text{ N}$  of  $+0.24 \pm 0.22\text{ yr}$

per decade ( $1\sigma$ -uncertainty level) for the 24 to 35 km altitude range for 1975–2005. This trend together with its valid altitude range and its  $2\sigma$ -uncertainty is marked as big black cross in Fig. 7. For better illustration the same picture with the MIPAS linear trend profiles for the two relevant latitude bins is shown in Fig. 7, bottom panel. The MIPAS AoA trends of 30 to 40 and 40 to 50° N are slightly lower than in the previous version and match now impressively well with the trend estimated by Engel et al. (2009) in the 24 to 35 km altitude region. One has to keep in mind, that the trend derived by Engel et al. (2009) represents the time period 1975–2005, while MIPAS measured from 2002 to 2012. So there is only a small time overlap between the two trends. Still the agreement of both is remarkable. The MIPAS AoA trends for the latitude bins 30 to 40 and 40 to 50° N are significantly distinct from zero for all altitudes above 22 km even on the  $2\sigma$ -uncertainty level.

## 5.2 Annual cycle and QBO influence

Figure 8 shows the amplitudes and phases of the seasonal cycle, i.e. the amplitudes and phases of terms with period length 1 year determined with the regression model described above. Compared to Figure 9 in Stiller et al. (2012) there are no substantial differences in the new data set. Thus, their respective conclusions remain valid in the light of the new data. Here we want to highlight the few differences and continue with the discussion, in particular by comparing the results with findings of other studies.

Diallo et al. (2012) found polar stratospheric AoA above 25 km, with youngest air at the end of local winter to spring, to be in the opposite phase than in the lowermost extra-tropical stratosphere in their analysis of ERA Interim data. In the model analysis of Li et al. (2012) the maximum of AoA in the polar region in spring is also bounded to the lower stratosphere whereas the upper polar stratosphere exhibits younger age. In contrast oldest air in Northern polar regions is found in MIPAS data in spring in the lower stratosphere and in mid-winter in the higher stratosphere. This difference to MIPAS AoA can be explained by the different derivations of AoA in the respective studies: while in Diallo et al. (2012) AoA is explicitly calculated by backward trajectories of the air parcel, and in Li et al. (2012) the AoA is determined by the pulse tracer method, the MIPAS AoA is derived by  $\text{SF}_6$  observations which exhibit an overaging when  $\text{SF}_6$  depleted mesospheric air subsides into the polar stratosphere during winter. This overaging in the polar stratosphere during winter shifts the phase in the MIPAS data towards oldest air in polar mid-winter, when subsidence of mesospheric air is strongest.

Some discernible difference to the previous data set is that the band of high seasonal amplitudes in the Northern mid-latitudes is not visible anymore in the new distribution of amplitudes (Fig. 8, top panel). Instead there is a region in Northern mid-latitudes above 25 km, which exhibits also high amplitudes like the equivalent region in the Southern

hemisphere. A higher amplitude of the seasonal cycle is now also found in the extra-tropical Southern lowermost stratosphere (LMS). Hence, now both hemispheres show enhanced seasonal amplitudes in the extra-tropical LMS, which are tentatively attributed to the seasonality of the permeability of the subtropical jet (Stiller et al., 2012) and flooding of this region with old vortex air after the vortex breakdown at the end of winter and spring.

Consistently Diallo et al. (2012) found high amplitudes of the seasonal cycle in the Southern and Northern extra-tropical LMS. Most parts of both the Southern and Northern extra-tropical LMS reach their maximum in AoA at the end of local winter to spring in the MIPAS data set as well as in the analysis by Diallo et al. (2012). This hemispheric symmetry is a feature of the new MIPAS data set. Bönisch et al. (2009) found oldest AoA in the Northern LMS in April and youngest in October with in-situ measurements of  $\text{SF}_6$  and  $\text{CO}_2$  during the SPURT aircraft campaigns. MIPAS observed youngest air in hemispheric late summer to autumn when the mixing barrier in the subtropics is weakest and young air from the tropics is injected in this region, also referred to as “flushing” of the LMS (Hegglin and Shepherd, 2007). Also cross-tropopause isentropic mixing from the tropical troposphere in the extra-tropical LMS is enhanced during summer-early autumn when the subtropical jet is weak (Chen, 1995).

Model results of Li et al. (2012) of the seasonal variation of AoA also agree with MIPAS in the extra-tropical LMS.

In the Northern subtropical lower stratosphere an abrupt meridional phase shift of almost half a year occurs, which means that these air masses are well isolated by the subtropical jet. Equatorwards the air is oldest in summer, when the subtropical mixing barrier and the BDC are weakest and older air from the extra-tropics is mixed in. This process is also indicated in the Southern Hemisphere and these opposite phases between the subtropics and the extra-tropics are also observed in the model results of Li et al. (2012).

In the mid-latitudinal middle and upper stratosphere the air is youngest in local winter, when, according to the known seasonality of the Brewer–Dobson-Circulation, younger air is brought to higher latitudes more efficiently. The mixing barriers are partially visible by abrupt phase shifts in the month of minimum and maximum age, respectively: air masses in the polar vortex are well isolated from the rest of the hemisphere. The subtropical mixing barrier is visible in the Northern lower stratosphere at 30° N and is indicated in the upper stratosphere only in the plot of maximum age of Fig. 8. In the Southern Hemisphere the abrupt phase shifts seem to occur at 50–60° S and at 10–20° S.

In the tropics below approx. 28 km air is youngest in boreal winter, even in the Southern Hemisphere (except for altitude–latitude-bins below 20 km). The hemispheric difference is lower than expected, which was also noticed by Stiller et al. (2012). However, this minimum in AoA in the Southern tropics occurs approx. 2 month later in the new MIPAS data. In the Northern Hemisphere air is oldest in late sum-



mer, while it is oldest in austral spring to early summer in the Southern Hemisphere. Furthermore this maximum in AoA in the Southern tropics occurs 2 month earlier in the new MIPAS data set compared to the previous one.

The amplitude of the QBO signal in AoA is shown in Fig. 9 for all latitudes and altitudes under assessment. High amplitudes are found not only in the tropics but also in the upper stratosphere at mid-latitudes, whereas highest amplitudes were found in the upper polar stratosphere. We also find high amplitudes in the Northern lowermost stratosphere.

## 6 Comparison with model simulation

The MIPAS SF<sub>6</sub>-based AoA trends for 2002–2012 are compared with trends derived from SF<sub>6</sub> distributions calculated with the Karlsruhe Simulation Model of the Middle Atmosphere (KASIMA), see Kouker et al. (1999); Ruhnke et al. (1999); Reddmann et al. (2001, 2010) for a description of the model and some applications. Here we used the model in the configuration as described in Reddmann et al. (2001), but with a T42/L63 configuration corresponding to about  $2.84^\circ \times 2.84^\circ$  horizontal resolution and 63 vertical levels between 7 and 120 km. In addition, the model is nudged to ERA-Interim analyses below 1 hPa. SF<sub>6</sub> mixing ratio values were set at the lower boundary of the model in the troposphere using NOAA/ESRL data. Note, that the model includes the mesospheric loss of SF<sub>6</sub>, which is implemented in the model according to Reddmann et al. (2001). Previously, Stiller et al. (2008) showed that the apparent high mean age values in late polar stratospheric winter observed in MIPAS observations can only be reproduced by the model simulations when including mesospheric loss.

For the determination of the trend of SF<sub>6</sub> derived mean age of air in the model calculation, the SF<sub>6</sub> distributions were calculated on a pressure-latitude grid using 64 latitude bins. In each pressure-latitude bin monthly zonal averages of SF<sub>6</sub> were calculated together with their standard error of the mean. The vertical pressure coordinates have been converted to geometrical altitudes assuming an isothermal atmosphere with a scale height  $H$  of 7 km ( $z = -H \ln(p/p_0)$ ). Afterwards the monthly zonal means have been interpolated on the MIPAS altitude grid and binned in the MIPAS latitude bins. These regridded zonal SF<sub>6</sub> monthly means were sampled and converted to AoA in the same manner as it was done for the measured SF<sub>6</sub> values (see Sect. 4.1).

Figure 10 shows the distribution of age trends calculated with simulated SF<sub>6</sub> values from the KASIMA model in a latitude–altitude plane with consideration of empirical errors and autocorrelations.

The model results agree remarkably well with the empirical AoA trends: positive decadal trends are found in the upper polar stratosphere in both hemispheres and at Northern mid-latitudes around 20 to 25 km while negative trends are found in the tropics and Southern subtropics as well as

in the Southern lower and lowermost stratosphere at mid-latitudes and Southern polar region. The most pronounced negative trend is detected in the Southern tropics and subtropics around 25 to 30 km, whereas it is found around 25 km in the MIPAS measurements. At Northern mid-latitudes at about 25 to 30 km altitude a tongue of negative trend is modelled. While MIPAS detected still positive trends there, there is at least a local age trend minimum in this region in the MIPAS data. At first glance there seems to be no disagreement between MIPAS and KASIMA in this region, because negative trends in KASIMA are not significant there. However, one has to be careful with the significances when comparing MIPAS and KASIMA: KASIMA is a nudged model, i.e. in wide parts of the atmosphere it represents the real atmosphere. This implies that the atmospheric variability patterns of KASIMA and MIPAS which are responsible for the error of the multilinear model share certain components and therefore cannot be assumed as fully uncorrelated. Thus, this error characterizes the expected difference between the regression function and truth, however, it cannot necessarily account for the differences between MIPAS and KASIMA. For this comparison the trends without consideration of the model errors may be more adequate. These figures are attached in the supplement and show that the region of the “negative tongue” is significant in KASIMA, whereas it is significantly positive in MIPAS.

At high latitudes lower stratospheric trends are positive in the MIPAS but negative in the KASIMA data set. These trends are not significant for MIPAS, however, they are significant when comparing the respective figures of trends without consideration of the model error (see Figures in the supplement). So there is indeed a contradiction in this region, which is most likely due to the “overaging” effect, which is more pronounced in the measured data because KASIMA underestimates polar winter subsidence.

What is striking in Fig. 10 is the hemispheric asymmetry between significant negative trends in the Southern Hemisphere and significant positive trends in the Northern Hemisphere, which was also found in the MIPAS data. This hemispheric asymmetry was also noticed by Monge-Sanz et al. (2012) with the TOMCAT model and by Mahieu et al. (2014) with the SLIMCAT model and was later also confirmed by Ploeger et al. (2015) with the CLaMS model.

## 7 Summary and conclusions

In this work the SF<sub>6</sub> retrieval setup for MIPAS ENVISAT spectra has been improved over the one developed by Stiller et al. (2012) and a newer version of spectra provided by ESA (level 1b data, version 5.02/5.06) was used to retrieve global profiles of the trace gas SF<sub>6</sub>. Monthly zonal means were converted in AoA using a tropospheric reference curve. The new AoA data set resembles roughly that of Stiller et al. (2012) but shows differences with respect to several details. Some

spurious features of the old data set no longer appear in the new data set. In particular, the new data set does not show the local AoA minimum at 36 km in the tropics, which was believed to be a retrieval artefact of the previous version and could be eliminated by a refined consideration of continuum radiation. A possible high bias of the old AoA data set above 40 km is removed as the air is considerably younger in this altitude region in the new data version.

The latitudinal cross-section of AoA at 20 km was compared to airborne observations from the 1990s and no substantial differences to the previous version of Stiller et al. (2012) were found. The comparison of AoA profiles with airborne measurements yields that in the tropics MIPAS AoA is older at all altitudes. At Northern mid-latitudes MIPAS agrees with most of SF<sub>6</sub> in-situ data whereas at high Northern latitudes MIPAS is again older, only the SF<sub>6</sub> air samples inside the polar vortex match with the MIPAS data.

The temporal variability of AoA over the 10 years of MIPAS measurements (2002–2012) was analysed by fitting a regression model to the AoA timeseries. The annual cycle in AoA of particular regions in the stratosphere was investigated and found to be in good agreement with other studies.

The derived AoA decadal trends show a pronounced hemispheric asymmetry above the lowermost stratosphere. The results of Stiller et al. (2012) were confirmed with respect to the typical values and the general morphology. The overall picture of linear increase/decrease in the latitude–altitude plane, however, is more contiguous and less patchy with the new data. Positive linear trends were confirmed for the Northern mid-latitudes and Southern polar middle stratosphere whereas negative trends were confirmed for the lowermost tropical stratosphere and lowermost Southern mid-latitudinal stratosphere. Differences to the previous data set occur in the Northern polar upper stratosphere, where trends are now positive, and in the middle tropical stratosphere, where trends are now negative. The latter might be explained by the removal of the retrieval artefact which changed the shape of the AoA profile in the tropics considerably. The linear increase in the Southern and Northern polar stratosphere and in the Northern mid-latitudes can be considered as robust results. The significant positive trend in the Northern mid-latitudes supports the findings of Engel et al. (2009) and the inferred trends match impressively well with the estimated trend by Engel et al. (2009).

The refined MIPAS observations on AoA in this study do not corroborate the results of various model studies, which consistently predict a decreasing AoA for the whole stratosphere. However, our decadal trends cannot be compared to results from long-term model studies. Our comparison with the KASIMA model for the period 2002–2012 shows, that the linear increase in the upper polar stratosphere and in the Northern mid-latitudes can be reproduced in the model at least when data is sampled and analysed in the same manner as the MIPAS data. It also demonstrates that the ERA-Interim data, used to nudge KASIMA, apparently are able to repro-

duce the observed transport trend, which shows that they are suitable for studies of the BDC and its trends.

Nevertheless this study finds a decreasing AoA trend in the tropics and in the lower and lowermost mid-latitudinal Southern stratosphere in agreement with long-term model studies, and hence supports the idea of an increasing shallow branch of the BDC, which was also proposed by Bönisch et al. (2011) and supported by Diallo et al. (2012), at least in the Southern Hemisphere.

**Acknowledgements.** This work was funded by the “CAWSES” priority programme of the German Research Foundation (DFG) under project STI 210/5-3 and by the German Federal Ministry of Education and Research (BMBF) within the “ROMIC” programme under project 01LG1221B.

E. Eckert was funded by the DFG project CL 319/2-1 (COLIBRI). We would like to acknowledge provision of MIPAS level-1b data by ESA and the SF<sub>6</sub> data from the NOAA/ESRL halocarbons in-situ programme. The authors also acknowledge support by Deutsche Forschungsgemeinschaft and Open Access Publishing Fund of Karlsruhe Institute of Technology.

The article processing charges for this open-access publication were covered by a Research Centre of the Helmholtz Association.

## References

- Andrews, A. E., Boering, K. A., Daube, B. C., Wofsy, S. C., Loewenstein, M., Jost, H., Podolske, J. R., Webster, C. R., Herman, R. L., Scott, D. C., Flesch, G. J., Moyer, E. J., Elkins, J. W., Dutton, G. S., Hurst, D. F., Moore, F. L., Ray, E. A., Romashkin, P. A., and Strahan, S. E.: Mean ages of stratospheric air derived from in situ observations of CO<sub>2</sub>, CH<sub>4</sub>, and N<sub>2</sub>O, *J. Geophys. Res.*, 106, 32295–32314, doi:10.1029/2001JD000465, 2001.
- Austin, J. and Li, F.: On the relationship between the strength of the Brewer–Dobson circulation and the age of stratospheric air, *Geophys. Res. Lett.*, 33, L17807, doi:10.1029/2006GL026867, 2006.
- Boering, K. A., Wofsy, S. C., Daube, B. C., Schneider, H. R., Loewenstein, M., Podolske, J. R., and Conway, T. J.: Stratospheric mean ages and transport rates from observations of carbon dioxide and nitrous oxide, *Science*, 274, 1340–1343, doi:10.1126/science.274.5291.1340, 1996.
- Bönisch, H., Engel, A., Curtius, J., Birner, Th., and Hoor, P.: Quantifying transport into the lowermost stratosphere using simultaneous in-situ measurements of SF<sub>6</sub> and CO<sub>2</sub>, *Atmos. Chem. Phys.*, 9, 5905–5919, doi:10.5194/acp-9-5905-2009, 2009.
- Bönisch, H., Engel, A., Birner, Th., Hoor, P., Tarasick, D. W., and Ray, E. A.: On the structural changes in the Brewer–Dobson circulation after 2000, *Atmos. Chem. Phys.*, 11, 3937–3948, doi:10.5194/acp-11-3937-2011, 2011.
- Bunzel, F. and Schmidt, H.: The brewer–dobson circulation in a changing climate: impact of the model configuration, *J. Atmos. Sci.*, 70, 1437–1455, 2013.

- Butchart, N.: The Brewer–Dobson Circulation, *Rev. Geophys.*, 52, 157–184, doi:10.1002/2013RG000448, 2014.
- Butchart, N. and Scaife, A. A.: Removal of chlorofluorocarbons by increased mass exchange between the stratosphere and troposphere in a changing climate, *Nature*, 410, 799–802, doi:10.1038/35071047, 2001.
- Butchart, N., Scaife, A. A., Bourqui, M., de Grandpre, J., Hare, S. H. E., Kettleborough, J., Langematz, U., Manzini, E., Sassi, F., Shibata, K., Shindell, D., and Sigmond, M.: Simulations of anthropogenic change in the strength of the Brewer–Dobson circulation, *Clim. Dynam.*, 27, 727–741, doi:10.1007/s00382-006-0162-4, 2006.
- Butchart, N., Cionni, I., Eyring, V., Shepherd, T. G., Waugh, D. W., Akiyoshi, H., Austin, J., Brühl, C., Chipperfield, M. P., Cordero, E., Dameris, M., Deckert, R., Dhomse, S., Frith, S. M., Garcia, R. R., Gettelman, A., Giorgetta, M. A., Kinnison, D. E., Li, F., Mancini, E., McLandress, C., Pawson, S., Pitari, G., Plummer, D. A., Rozanov, E., Sassi, F., Scinocca, J. F., Shibata, K., Steil, B., and Tian, W.: Chemistry–climate model simulations of twenty-first century stratospheric climate and circulation changes, *J. Climate*, 23, 5349–5374, 2010.
- Calvo, N. and Garcia, R. R.: Wave forcing of the tropical upwelling in the lower stratosphere under increasing concentrations of greenhouse gases, *J. Atmos. Sci.*, 66, 3184–3196, 2009.
- Chen, P.: Isentropic cross-tropopause mass exchange in the extratropics, *J. Geophys. Res.-Atmos.*, 100, 16661–16673, doi:10.1029/95JD01264, 1995.
- Diallo, M., Legras, B., and Chédin, A.: Age of stratospheric air in the ERA-Interim, *Atmos. Chem. Phys.*, 12, 12133–12154, doi:10.5194/acp-12-12133-2012, 2012.
- Douglass, A. R., Stolarski, R. S., Schoeberl, M. R., Jackman, C. H., Gupta, M. L., Newman, P. A., Nielsen, J. E., and Fleming, E. L.: Relationship of loss, mean age of air and the distribution of CFCs to stratospheric circulation and implications for atmospheric lifetimes, *J. Geophys. Res.*, 113, D14309, doi:10.1029/2007JD009575, 2008.
- Engel, A., Möbius, T., Bönisch, H., Schmidt, U., Heinz, R., Levin, I., Atlas, E., Aoki, S., Nakazawa, T., Sugawara, S., Moore, F., Hurst, D., Elkins, J., Schauffler, S., Andrews, A., and Boering, K.: Age of stratospheric air unchanged within uncertainties over the past 30 years, *Nature Geosci.*, 2, 28–31, doi:10.1038/ngeo388, 2009.
- Fischer, H., Blom, C., Oelhaf, H., Carli, B., Carlotti, M., Delbouille, L., Ehrt, D., Flaud, J.-M., Isaksen, I., López-Puertas, M., McElroy, C. T., and Zander, R.: Envisat-MIPAS, an instrument for atmospheric chemistry and climate research, European Space Agency-Report SP-1229, edited by: Readings C. and Harris R. A., ESA Publications Division, ESTEC, P.O. Box 299, 2200 AG Noordwijk, the Netherlands, 2000.
- Fischer, H., Birk, M., Blom, C., Carli, B., Carlotti, M., von Clarmann, T., Delbouille, L., Dudhia, A., Ehrt, D., Endemann, M., Flaud, J. M., Gessner, R., Kleinert, A., Koopman, R., Langen, J., López-Puertas, M., Mosner, P., Nett, H., Oelhaf, H., Perron, G., Remedios, J., Ridolfi, M., Stiller, G., and Zander, R.: MIPAS: an instrument for atmospheric and climate research, *Atmos. Chem. Phys.*, 8, 2151–2188, doi:10.5194/acp-8-2151-2008, 2008.
- Flaud, J.-M., Piccolo, C., Carli, B., Perrin, A., Coudert, L. H., Teffo, J.-L., and Brown, L. R.: Molecular line parameters for the MIPAS (Michelson Interferometer for Passive Atmospheric Sounding) experiment, *Atmos. Oceanic Opt.*, 16, 172–182, 2003.
- Funke, B. and Höpfner, M.: Non-LTE and radiative transfer, in: The Karlsruhe Optimized and Precise Radiative Transfer Algorithm (KOPRA), edited by: Stiller, G. P., Wissenschaftliche Berichte FZKA 6487, Forschungszentrum Karlsruhe, Karlsruhe, 101–106, 2000.
- Funke, B., López-Puertas, M., Gil-López, S., von Clarmann, T., Stiller, G. P., Fischer, H., and Kellmann, S.: Downward transport of upper atmospheric NO<sub>x</sub> into the polar stratosphere and lower mesosphere during the Antarctic 2003 and Arctic 2002/2003 winters, *J. Geophys. Res.*, 110, D24308, doi:10.1029/2005JD006463, 2005.
- Funke, B., López-Puertas, M., Bermejo-Pantaleón, D., von Clarmann, T., Stiller, G. P., Höpfner, M., Grabowski, U., and Kaufmann, M.: Analysis of nonlocal thermodynamic equilibrium CO 4.7 μm fundamental, isotopic and hot band emissions measured by the Michelson Interferometer for Passive Atmospheric Sounding on Envisat, *J. Geophys. Res.*, 112, D11305, doi:10.1029/2006JD007933, 2007.
- Garcia, R. R. and Randel, W. J.: Acceleration of the Brewer–Dobson circulation due to increases in greenhouse gases, *J. Atmos. Sci.*, 65, 2731–2739, doi:10.1175/2008JAS2712.1, 2008.
- Hall, B. D., Dutton, G. S., Mondeel, D. J., Nance, J. D., Rigby, M., Butler, J. H., Moore, F. L., Hurst, D. F., and Elkins, J. W.: Improving measurements of SF<sub>6</sub> for the study of atmospheric transport and emissions, *Atmos. Meas. Tech.*, 4, 2441–2451, doi:10.5194/amt-4-2441-2011, 2011.
- Hall, T. M. and Plumb, R. A.: Age as a diagnostic of stratospheric transport, *J. Geophys. Res.*, 99, 1059–1070, 1994.
- Hall, T. M., Waugh, D. W., Boering, K. A., and Plumb, R. A.: Evaluation of transport in stratospheric models, *J. Geophys. Res.*, 104, 18815–18839, 1999.
- Harnisch, J., Borchers, R., Fabian, P., and Maiss, M.: Tropospheric trends for CF<sub>4</sub> and C<sub>2</sub>F<sub>6</sub> since 1982 derived from SF<sub>6</sub> dated stratospheric air, *Geophys. Res. Lett.*, 23, 1099–1102, 1996.
- Hegglin, M. I. and Shepherd, T. G.: O<sub>3</sub>–N<sub>2</sub>O correlations from the atmospheric chemistry experiment: revisiting a diagnostic of transport and chemistry in the stratosphere, *J. Geophys. Res.*, 112, D19301, doi:10.1029/2006JD008281, 2007.
- Kouker, W., Offermann, D., Küll, V., Reddmann, T., Ruhnke, R., and Franzen, A.: Streamers observed by the CRISTA experiment and simulated in the KASIMA model, *J. Geophys. Res.*, 104, 16405–16418, 1999.
- Kyrölä, E., Tamminen, J., Sofieva, V., Bertaux, J. L., Hauchecorne, A., Dalaudier, F., Fussen, D., Vanhellemont, F., Fanton d’Andon, O., Barrot, G., Guirlet, M., Fehr, T., and Saavedra de Miguel, L.: GOMOS O<sub>3</sub>, NO<sub>2</sub>, and NO<sub>3</sub> observations in 2002–2008, *Atmos. Chem. Phys.*, 10, 7723–7738, doi:10.5194/acp-10-7723-2010, 2010.
- Li, F., Austin, J., and Wilson, J.: The strength of the brewer–dobson circulation in a changing climate: coupled chemistry–climate model simulations, *J. Climate*, 21, 40–57, 2008.
- Li, F., Stolarski, R. S., and Newman, P. A.: Stratospheric ozone in the post-CFC era, *Atmos. Chem. Phys.*, 9, 2207–2213, doi:10.5194/acp-9-2207-2009, 2009.
- Li, F., Waugh, D. W., Douglass, A. R., Newman, P. A., Pawson, S., Stolarski, R. S., Strahan, S. E., and Nielsen, J. E.: Seasonal variations of stratospheric age spectra in the Goddard Earth Observ-

- ing System Chemistry Climate Model (GEOSCCM), *J. Geophys. Res.-Atmos.*, 117, D05134, doi:10.1029/2011JD016877, 2012.
- Mahieu, E., Chipperfield, M. P., Notholt, J., Reddmann, T., Anderson, J., Bernath, P. F., Blumenstock, T., Coffey, M. T., Dhomse, S. S., Feng, W., Franco, B., Froidevaux, L., Griffith, D. W. T., Hannigan, J. W., Hase, F., Hossaini, R., Jones, N. B., Morino, I., Murata, I., Nakajima, H., Palm, M., Paton-Walsh, C., Russell III, J. M., Schneider, M., Servais, C., Smale, D., and Walker, K. A.: Recent Northern Hemisphere stratospheric HCl increase due to atmospheric circulation changes, *Nature*, 515, 104–107, 2014.
- McLandress, C. and Shepherd, T. G.: Simulated anthropogenic changes in the Brewer–Dobson circulation, including its extension to high latitudes, *J. Climate*, 22, 1516–1540, doi:10.1175/2008JCLI2679.1, 2009.
- Monge-Sanz, B. M., Chipperfield, M. P., Dee, D. P., Simmons, A. J. and Uppala, S. M.: Improvements in the stratospheric transport achieved by a chemistry transport model with ECMWF (re)analyses: identifying effects and remaining challenges. *Q.J.R. Meteorol. Soc.*, 139: 654–673. doi:10.1002/qj.1996, 2013.
- Neely III, R. R., English, J. M., Toon, O. B., Solomon, S., Mills, M., and Thayer, J. P.: Implications of extinction due to meteoritic smoke in the upper stratosphere, *Geophys. Res. Lett.*, 38, L24808, doi:10.1029/2011GL049865, 2011.
- Oberländer, S., Langematz, U., and Meul, S.: Unraveling impact factors for future changes in the Brewer–Dobson circulation, *J. Geophys. Res.-Atmos.*, 118, 10296–10312, doi:10.1002/jgrd.50775, 2013.
- Okamoto, K., Sato, K., and Akiyoshi, H.: A study on the formation and trend of the Brewer–Dobson circulation, *J. Geophys. Res.-Atmos.*, 116, D10117, doi:10.1029/2010JD014953, 2011.
- Ploeger, F., Riese, M., Haenel, F., Konopka, P., Müller, R. and Stiller, G.: Variability of stratospheric mean age of air and of the local effects of residual circulation and eddy mixing, *J. Geophys. Res. Atmos.*, 120, 716–733, doi:10.1002/2014JD022468, 2015.
- Randel, W. J., Wu, F., Vömel, H., Nedoluha, G. E., and Forster, P.: Decreases in stratospheric water vapor after 2001: links to changes in the tropical tropopause and the Brewer–Dobson circulation, *J. Geophys. Res.*, 111, D12312, doi:10.1029/2005JD006744, 2006.
- Ray, E. A., Moore, F. L., Elkins, J. W., Dutton, G. S., Fahey, D. W., Vömel, H., Oltmans, S. J., and Rosenlof, K. H.: Transport into the Northern Hemisphere lowermost stratosphere revealed by in situ tracer measurements, *J. Geophys. Res.*, 104, 26565–26580, doi:10.1029/1999JD900323, 1999.
- Reddmann, T., Ruhnke, R., and Kouker, W.: Three-dimensional model simulations of SF<sub>6</sub> with mesospheric chemistry, *J. Geophys. Res.*, 106, 14525–14537, doi:10.1029/2000JD900700, 2001.
- Reddmann, T., Ruhnke, R., Versick, S., and Kouker, W.: Modeling disturbed stratospheric chemistry during solar-induced NO<sub>x</sub> enhancements observed with MIPAS/ENVISAT, *J. Geophys. Res.-Atmos.*, 115, D00I11, doi:10.1029/2009JD012569, 2010.
- Remedios, J. J., Leigh, R. J., Waterfall, A. M., Moore, D. P., Sembhi, H., Parkes, I., Greenhough, J., Chipperfield, M. P., and Hauglustaine, D.: MIPAS reference atmospheres and comparisons to V4.61/V4.62 MIPAS level 2 geophysical data sets, *Atmos. Chem. Phys. Discuss.*, 7, 9973–10017, doi:10.5194/acpd-7-9973-2007, 2007.
- Rind, D., Suozzo, R., Balachandran, N. K., and Prather, M. J.: Climate change and the middle atmosphere. part i: the doubled CO<sub>2</sub> climate, *J. Atmos. Sci.*, 47, 465–494, 1990.
- Rothman, L. S., Barbe, A., Benner, D. C., Brown, L. R., Camy-Peyret, C., Carleer, M. R., Chance, K., Clerbaux, C., Dana, V., Devi, V. M., Fayt, A., Flaud, J.-M., Gamche, R. R., Goldman, A., Jacquemart, D., Jucks, K. W., Lafferty, W. J., Mandin, J.-Y., Massie, S. T., Nemtchinov, V., Newnham, D. A., Perrin, A., Rinsland, C. P., Schroeder, J., Smith, K. M., Smith, M. A. H., Tang, K., Toth, R. A., Vander Auwera, J., Varanasi, P., and Yoshino, K.: The HITRAN molecular spectroscopic database: edition of 2000 including updates through 2001, *J. Quant. Spectrosc. Ra.*, 82, 5–44, doi:10.1016/S0022-4073(03)00146-8, 2003.
- Ruhnke, R., Kouker, W., and Reddmann, T.: The influence of the OH + NO<sub>2</sub> + M reaction on the NO<sub>y</sub> partitioning in the late Arctic winter 1992/1993 as studied with KASIMA, *J. Geophys. Res.*, 104, 3755–3772, 1999.
- Shepherd, T. G.: Dynamics, stratospheric ozone, and climate change, *Atmos. Ocean*, 46, 117–138, doi:10.3137/ao.460106, 2008.
- SPARC CCMVal: Neu, J. and Strahan, S., Chapter 5. Transport, in: *SPARC Report on the Evaluation of Chemistry-Climate Models*, edited by: Eyring, V., Shepherd, T. G., and Waugh, D. W., SPARC Report No. 5, WCRP-132, WMO/TD-No. 1526, available at: <http://www.atmosp.physics.utoronto.ca/SPARC>, SPARC/WMO, Zurich, 2010.
- Stiller, G. P. (Ed.): *The Karlsruhe Optimized and Precise Radiative Transfer Algorithm (KOPRA)*, vol. FZKA 6487 of Wissenschaftliche Berichte, Forschungszentrum Karlsruhe, 2000.
- Stiller, G. P., von Clarmann, T., Funke, B., Glatthor, N., Hase, F., Höpfner, M., and Linden, A.: Sensitivity of trace gas abundances retrievals from infrared limb emission spectra to simplifying approximations in radiative transfer modelling, *J. Quant. Spectrosc. Ra.*, 72, 249–280, 2002.
- Stiller, G. P., von Clarmann, T., Höpfner, M., Glatthor, N., Grabowski, U., Kellmann, S., Kleinert, A., Linden, A., Milz, M., Reddmann, T., Steck, T., Fischer, H., Funke, B., López-Puertas, M., and Engel, A.: Global distribution of mean age of stratospheric air from MIPAS SF<sub>6</sub> measurements, *Atmos. Chem. Phys.*, 8, 677–695, doi:10.5194/acp-8-677-2008, 2008.
- Stiller, G. P., von Clarmann, T., Haenel, F., Funke, B., Glatthor, N., Grabowski, U., Kellmann, S., Kiefer, M., Linden, A., Lossow, S., and López-Puertas, M.: Observed temporal evolution of global mean age of stratospheric air for the 2002 to 2010 period, *Atmos. Chem. Phys.*, 12, 3311–3331, doi:10.5194/acp-12-3311-2012, 2012.
- Tikhonov, A.: On the solution of incorrectly stated problems and method of regularization, *Dokl. Akad. Nauk. SSSR*, 151, 501–504, 1963.
- von Clarmann, T., Glatthor, N., Grabowski, U., Höpfner, M., Kellmann, S., Kiefer, M., Linden, A., Mengistu Tsidu, G., Milz, M., Steck, T., Stiller, G. P., Wang, D. Y., Fischer, H., Funke, B., Gil-López, S., and López-Puertas, M.: Retrieval of temperature and tangent altitude pointing from limb emission spectra recorded from space by the Michelson Interferometer for Passive Atmospheric Sounding (MIPAS), *J. Geophys. Res.*, 108, 4736, doi:10.1029/2003JD003602, 2003.
- von Clarmann, T., Höpfner, M., Kellmann, S., Linden, A., Chauhan, S., Funke, B., Grabowski, U., Glatthor, N., Kiefer, M., Schiefer-

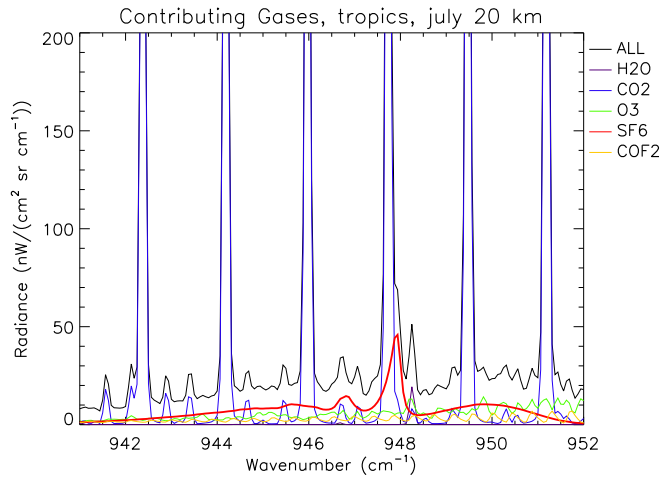


**Figure 1.** Contributing trace gases to a typical spectrum measured at mid-latitudes in July at 20 km (low resolution) with the SF<sub>6</sub> signature in red.

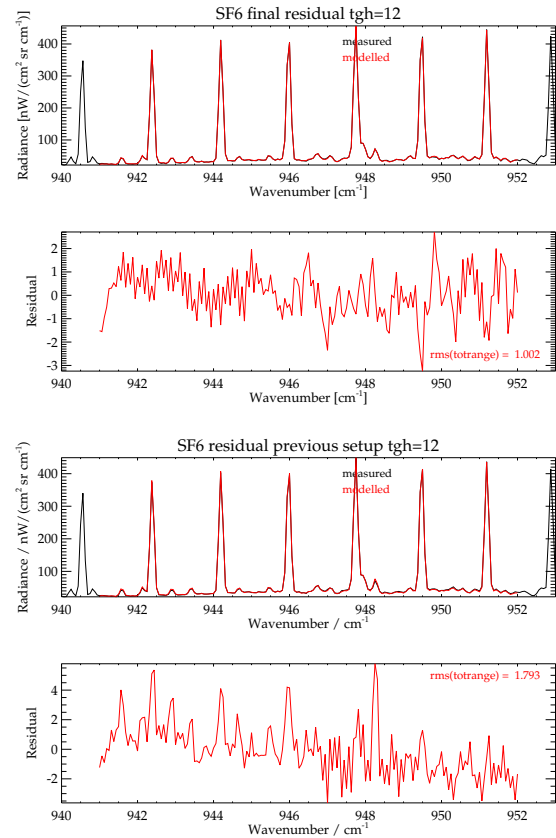


**Figure 2.** Coadded spectra (measured and modelled) and residuals for tangent height 12 (approx. 24 km) over one day for the final retrieval setup (upper panels) and for the the previous retrieval setup (lower panels).

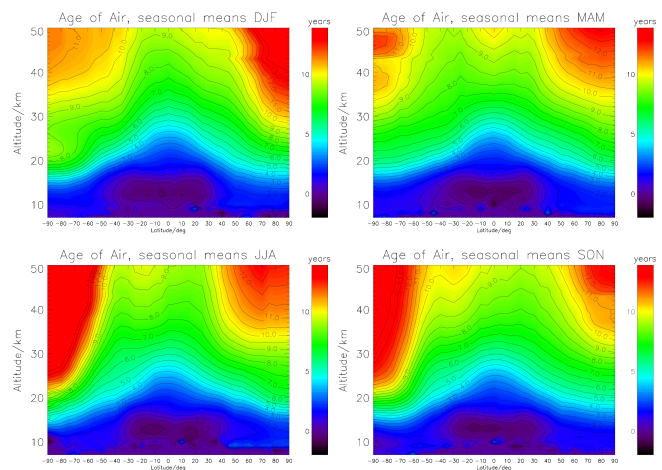


**Figure 3.** Zonal mean distribution of mean age of stratospheric air for the four seasons, derived by averaging MIPAS AoA data of all available years for the respective season.

- 1205 decker, T., Stiller, G. P., and Versick, S.: Retrieval of temperature, H<sub>2</sub>O, O<sub>3</sub>, HNO<sub>3</sub>, CH<sub>4</sub>, N<sub>2</sub>O, ClONO<sub>2</sub> and ClO from MIPAS reduced resolution nominal mode limb emission measurements, *Atmos. Meas. Tech.*, 2, 159–175, doi:10.5194/amt-2-159-2009, 2009.
- 1210 von Clarmann, T., Stiller, G., Grabowski, U., Eckert, E., and Orphal, J.: Technical Note: Trend estimation from irregularly sampled, correlated data, *Atmos. Chem. Phys.*, 10, 6737–6747, doi:10.5194/acp-10-6737-2010, 2010.
- 1215 Waugh, D. W. and Hall, T. M.: Age of stratospheric air: theory, observations, and models, *Rev. Geophys.*, 40, 1010, doi:10.1029/2000RG000101, 2002.

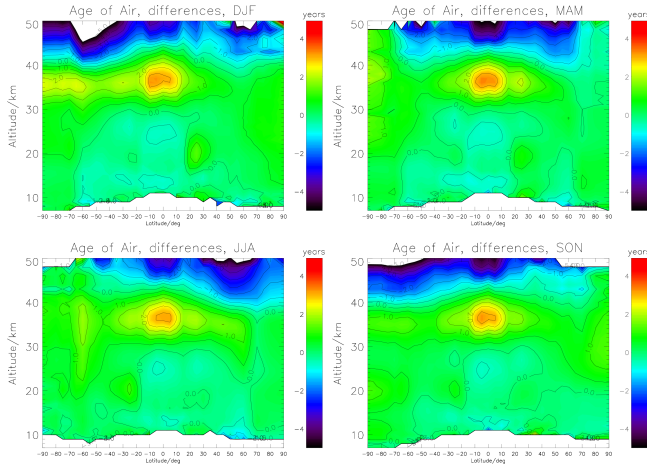


**Figure 4.** Differences of zonal seasonal mean distribution of mean age of stratospheric air to the previous data version averaged for the four seasons.

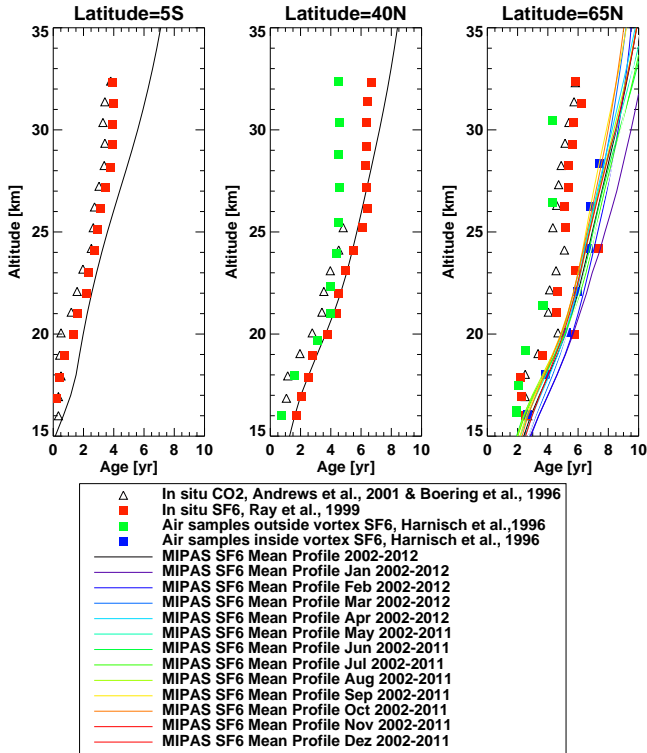


**Figure 5.** Comparison of MIPAS AoA profiles with airborne profiles of the 1990s for the tropics (5° S), the Northern mid-latitudes (40° N) and the Northern high latitudes (65° N).

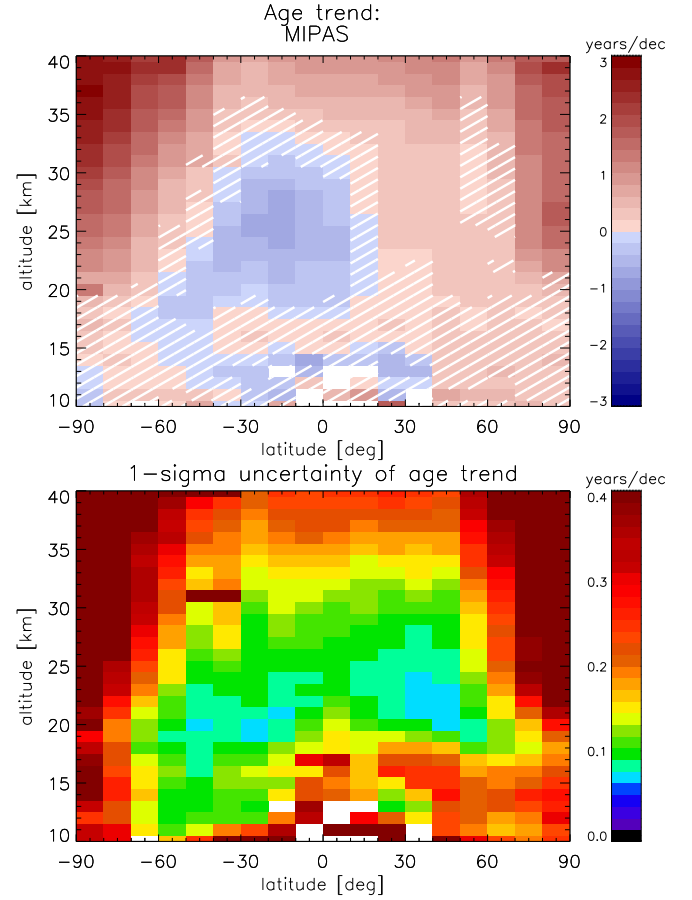


**Figure 6.** Top: Altitude–latitude cross-section of the model-error corrected linear increase of MIPAS AoA over the years 2002 to 2012, i.e. after including the model error and autocorrelations between the data points in the fit. Hatched areas indicate where the trend is not significant, i.e. it is smaller (in absolute terms) than its  $2\sigma$ -uncertainty. Bottom:  $1\sigma$ -uncertainty of the trend in terms of years/decade.

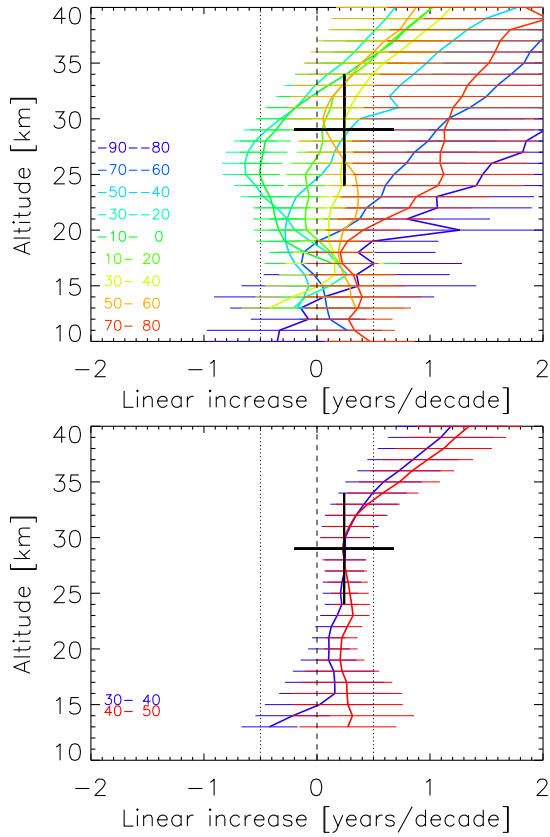


**Figure 7.** Vertical profiles of the age of air linear increase/decrease over the years 2002 to 2012 for example latitudes. Horizontal bars give the  $2\sigma$ -uncertainties of the linear variations. The 30 yr trend as derived by Engel et al. (2009) for the Northern mid-latitudes is also shown for comparison as a black cross indicating its valid altitude range and its  $2\sigma$ -uncertainty.

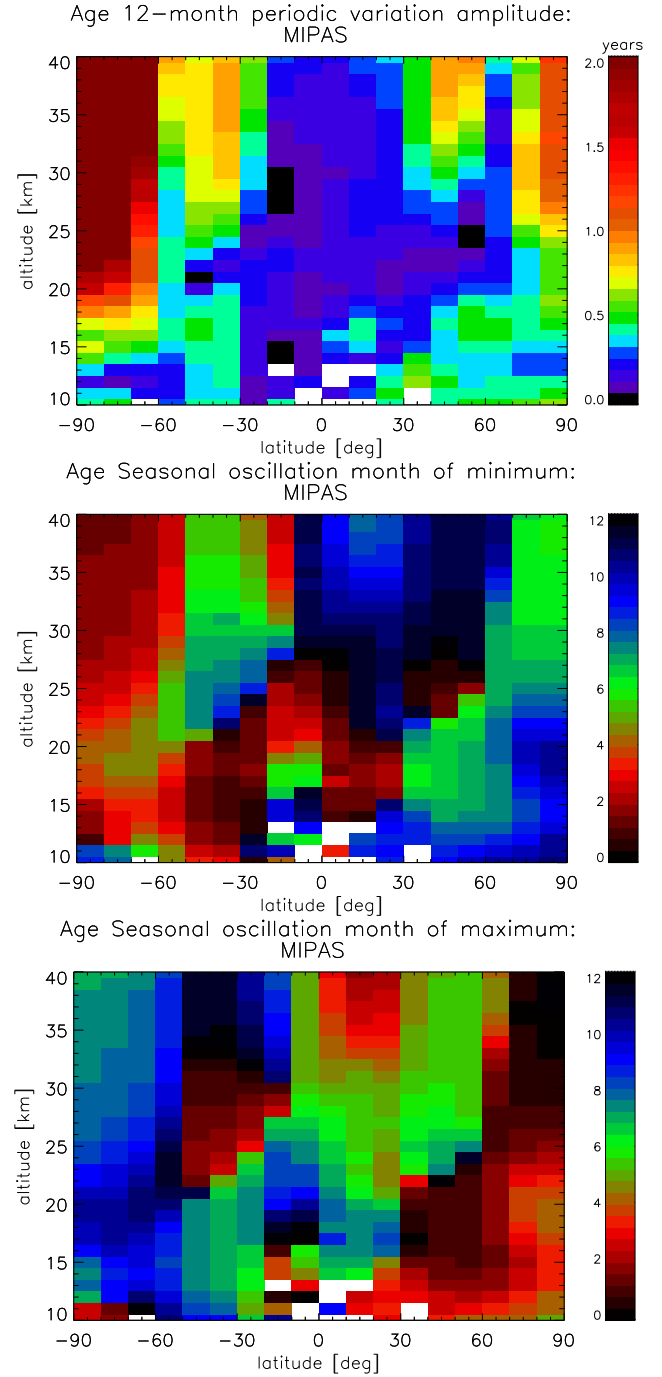


**Figure 8.** Altitude–latitude cross-sections of amplitudes (top) and month of the minimum (middle) and maximum (bottom) of the seasonal variation of mean age of air.

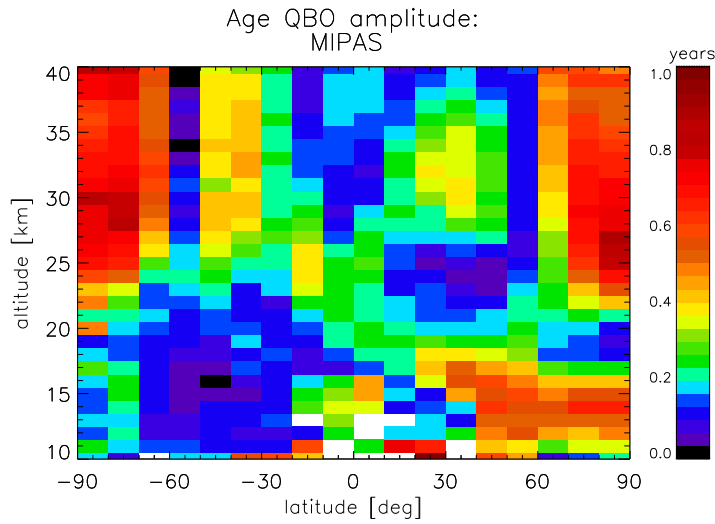


**Figure 9.** Altitude–latitude cross-sections of amplitudes of the QBO-variation of mean age of air.

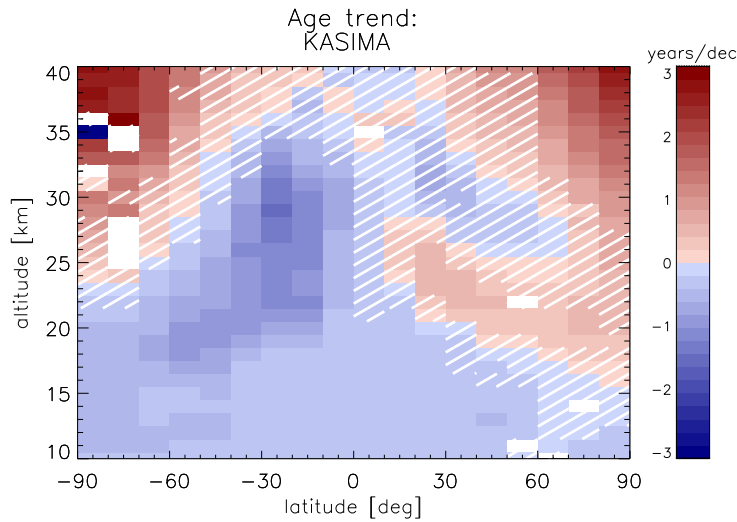


**Figure 10.** Calculated AoA trends for 2002–2012 from the KASIMA model with consideration of empirical errors and auto-correlation. Hatched areas indicate where the trend is not significant.